CHEMISTRY OF MATERIALS

Article

pubs.acs.org/cm

Shell or Dots – Precursor Controlled Morphology of Au–Se Deposits on CdSe Nanoparticles

Leonor de la Cueva,[†,¶] Michaela Meyns,[‡,∇,¶] Neus G. Bastús,[§] Jonathan Rodríguez-Fernández,[∥] Roberto Otero,[†,∥] José M. Gallego,[†,⊥] Concepción Alonso,[#] Christian Klinke,[*,‡] and Beatriz H. Juárez[*,†,#]

[†]Madrid Institute of Advanced Studies in Nanoscience, IMDEA Nanoscience, Faraday 9, Cantoblanco, 28049 Madrid, Spain

[‡]Institute of Physical Chemistry, University of Hamburg, Grindelallee 117, 20146 Hamburg, Germany

[§]Institut Català de Nanociència i Nanotecnologia (ICN2), CSIC and The Barcelona Institute of Science and Technology, Campus UAB, Bellaterra, 08193 Barcelona, Spain

[∥]Physics Condense Matter Department, Universidad Autónoma de Madrid, 28049 Madrid, Spain

[⊥]Instituto de Ciencia de Materiales de Madrid, Consejo Superior de Investigaciones Científicas (ICMM-CSIC), Sor Juana Inés de la Cruz 3, Cantoblanco, 28049 Madrid, Spain

[#]Department of Applied Physical Chemistry, Universidad Autónoma de Madrid, Cantoblanco, 28049 Madrid, Spain

Supporting Information

ABSTRACT: The most prevalent image of the morphology of Au–CdSe hybrid nanoparticles (HNPs) is that of dumbbells or matchsticks with CdSe nanoparticles (NPs) acting as seed material onto which spherical Au dots are deposited. On the basis of a system with only three reaction components, CdSe seeds, *n*-dodecyltrimethylammonium bromide-complexed $AuCl_3$, and dodecanethiol, we demonstrate how the morphology of the Au deposits on the semiconductor NPs, either in the form of dots on the vertices or in the form of a shell around the NP surface, can be determined by controlling the oxidation state of the metal precursor. Furthermore, we apply X-ray photoelectron spectroscopy to show that the resultant deposits are composed of partially oxidized Au, corresponding to a Au–Se compound regardless the deposit morphology. To obtain a detailed characterization of the HNPs with different morphologies and to gain mechanistic insights into the deposition process, (cryogenic) high-resolution transmission electron microscopy, mass spectrometry, cyclic voltammetry, and computational simulations have been performed. Our results emphasize that the knowledge of the surface chemistry of the seed particles as well as a defined picture of the metal precursors is necessary to understand heterodeposition processes.

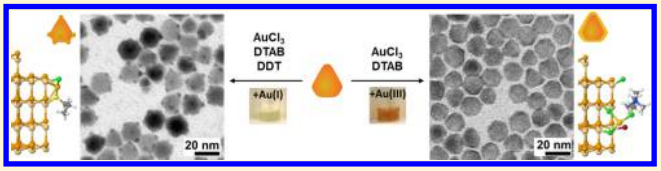

INTRODUCTION

The small dimensions and the high chemical reactivity of nanoparticles (NPs) have opened the door to a whole universe of new material combinations, compositions, and architectures. The growth of multidomain semiconductor–metal hybrid nanoparticles (HNPs) by colloidal seeded-growth techniques (consisting essentially of the reduction of a metal complex on the surface of semiconductor NPs used as a seeds) has attracted particular interest.[1−4] By taking advantage of the different surface chemistries of the two components, metallic domains can act as anchor points for biofunctionalization or help to direct the self-assembly of the HNPs.[5,6] With respect to the physical properties, the growth of Au or Pt metallic contacts on individual semiconducting CdSe NPs increases their conductance and enables charge separation of generated electron–hole pairs, finding applications in photocatalysis and hydrogen generation.[7−14] The reduction process of the metal precursor depends on the surface chemistry of the semiconductor seeds, including for example the presence of polar or nonpolar facets, the type of atoms, dangling bonds, etc.[15,16] Besides, the interaction of the precursor with ligands having different length and ligand density on a particular facet and, especially, the oxidation state of the precursor and its concentration play important roles.[17,18] In general, the reduction of metal complexes in organic media results in elemental metal deposits, as in the case of phosphonic acid-capped CdSe, which are held responsible for increasing the electrical conductivity in the final HNPs.[19] In most cases the metallic deposits grow exclusively in the form of spherical dots, on the tips, apexes, or defects on the different NP facets.[6,15,20]

While a commonly applied strategy involving a mixture of $AuCl_3$, a complex agent in the form of alkylammonium bromides, and alkylamines as mild reducing agent frequently results in dumbbell or matchstick-like morphologies with CdSe (or CdS) nanorods as the center domain,[6,20] a distinctly different behavior was observed with hexagonal pyramidal CdSe NPs.[17] Instead of well-defined and stable spherical Au domains, a shell-like structure that evolved into irregular Au dots upon exposure to the electron beam during transmission electron microscopy (TEM) inspections was observed. The possibility

Received: January 21, 2016
Revised: March 31, 2016
Published: March 31, 2016

DOI: 10.1021/acs.chemmater.6b00287
Chem. Mater. 2016, 28, 2704−2714

to precisely adjust the final morphology of the Au domain (either shell or dots) by selectively adding strong reducing agents to the reaction solution suggested that the change of the HNP morphology during TEM inspection was due to an observer problem—the interaction with the electron beam, ultimately modifying its oxidation state.[30,44−46]

With the present work we seek to show that the question of whether dots or a shell are formed during Au deposition not only is grounded on an observer effect or postsynthetic reduction. By slightly varying the synthetic protocol, in particular the oxidation state of the Au precursor, we are able to demonstrate control over the morphology of the Au deposits in HNPs. On the seed side, the particular morphology and surface chemistry of pyramidal wurtzite CdSe NPs also comes into play. CdSe nanorods are usually capped by a high density of long-alkyl chain phosphonic acid-related molecules and exhibit large facets terminated by both elements of the crystal. Pyramidal NPs can be obtained through ripening of the rods in a chlorinated medium.[21−24] This procedure gives NPs capped by a mixed ligand sphere with a relatively low density of phosphonic acid-related molecules and chloride ions.[25,26] Furthermore, {101} planes terminated either by Cd or Se are favored.[24] Our aim in this paper is to understand the mechanistic aspects of Au deposition and to identify differences in the nature of the Au deposits, which we found not to be elemental Au but Au in a higher oxidation state. To this aim, we investigated the role of all reactants and applied a comprehensive combination of analytical tools such as (cryogenic) high-resolution electron microscopy (HR-TEM), X-ray photoelectron spectroscopy (XPS), mass spectrometry (MS), X-ray diffraction (XRD), and cyclic voltammetry (CV) in combination with computational modeling.

EXPERIMENTAL METHODS

Materials. Cadmium oxide (CdO; 99.99%) was bought from ChemPur. Tri-*n*-octylphosphane (TOP; 90%, stored in a nitrogen filled glovebox), 1-chlorooctadecane (ODC; 96%), selenium shots (amorphous, 2−4 mm, 0.08−0.16 in., 99.999%, stored in a nitrogen filled glovebox), gold(III) chloride ($AuCl_3$; 99%, stored in a nitrogen filled glovebox), anhydrous acetonitrile (99.8%, stored in a nitrogen filled glovebox), and tetrabutylammonium perchlorate (TBAP; 99%) were purchased from Sigma-Aldrich. Tri-*n*-octylphosphane oxide (TOPO; > 98%), silver nitrate ($AgNO_3$; 99.8%), and toluene (p. A.) were obtained from Merck. Acros is the producer of 1-dodecanothiol (DDT; 98%), while *n*-dodecyltrimethylammonium bromide (DTAB; 99%, vacuum-dried and stored in a nitrogen filled glovebox) and *n*-octadecylphosphonic acid (ODPA; 97−98%) were acquired from Alfa Aesar. Highly oriented pyrolitic graphite (HOPG) substrates of ZYB quality (10 × 10 × 2 mm^3) and the glassy-carbon (GC) electrodes (ø1 × 15 mm) were bought from NT-MDT and HTW, respectively.

Preparation of CdSe NP Seed Solutions. The reactions were carried out under nitrogen atmosphere utilizing a Schlenk line. Pyramidal CdSe NPs were synthesized according to previous work with slight modifications.[21,24] A mixture of 25 mg of CdO (0.19 mmol), 0.14 g of ODPA (0.42 mmol), and 3.0 g of TOPO was heated to 120 °C under vacuum for 30 min, during which two switches to nitrogen were carried out. Then, the mixture was heated to 270−290 °C to form a colorless $Cd(ODPA)_2$ complex. Afterward, the temperature was set to 265 °C, and 43 μL (0.13 mmol) of 1-chlorooctadecane (ODC) were injected. After 25 min, 0.42 mL (0.42 mmol) of 1 M TOPSe were injected before reducing the temperature to 255 °C for growth. After 24 h, the reaction was quenched by cooling down to 75 °C and injecting 3.0 mL of toluene to prevent solidification. The NPs were purified by three cycles of precipitation and centrifugation at 1856*g*/4500 rpm and further redispersed in toluene/methanol (2:1). Of this solution, 100 μL were diluted to 3 mL in a quartz cuvette, and the optical density was determined at the crossing of the tangents of the first absorption maximum. Multiplied by 30, this value was taken for the optical density of the dispersion (OD_{CdSe}). For a seed solution an appropriate volume of the purified CdSe NP solution was diluted with toluene to reach a volume of 4 mL and an optical density of 0.27 (V_{CdSe} solution × OD_{CdSe}/4 mL).

Preparation of Au(III)-Stock Solution. A 4.4 mM Au(III)-stock solution was prepared by mixing gold(III) chloride (20 mg, 66 μmol) and *n*-dodecyltrimethylammonium bromide (DTAB, 32 mg, 104 μmol) in 15 mL of toluene in a nitrogen atmosphere. After mild sonication and slight warming (heating plate, 50 °C) a clear, orange-red solution was obtained. It was stored in darkness under ambient conditions until further use.

Synthesis of CdSe-Au HNPs. We added the Au solutions to CdSe seeds dispersed in 4 mL of toluene with an optical density of 0.27 at the first absorption maximum. Au solutions with different contents of Au were injected under stirring in ambient conditions. For easy comparison, the ratio Au/CdSe was defined as the molar amount (n) of Au in μmol divided by the product of volume CdSe stock solution and the optical density (V_{CdSe} solution × OD_{CdSe}) in substitution for the exact molar amount of CdSe. After the reactions, all samples were precipitated by centrifugation (3 min, 7000 rpm/4492*g*), separated from the supernatant, and redispersed in toluene three times. The first time, toluene/ethanol (1:1) was enough to precipitate the particles, and the second and third times methanol had to be used to provoke precipitation.

a. Au-Shell Deposition with Au(III)-Stock Solution. For shell deposition appropriate amounts of Au(III)-stock solution were diluted to 2.0 mL with toluene and added to the CdSe NP dispersion. To obtain a thin Au shell with a Au/CdSe = 2, 474 μL of the Au solution, containing 0.64 mg (2.1 μmol) of $AuCl_3$ and 0.96 mg (3.1 μmol) of DTAB, was injected. A thick Au shell with Au/CdSe = 2.9 was obtained with 684 μL of the Au solution containing 0.91 mg (3.0 μmol) of $AuCl_3$ and 1.5 mg (4.8 μmol) of DTAB. HNPs with a Au shell formed within 10 min and became instable in the solution in toluene. By adding dodecanethiol DDT (at least 18-fold with regard to Au) they can be stabilized again in the same solution and remain dispersible even after purification.

b. Au-Dot Deposition with Au(I)−DDT. To obtain different Au/CdSe ratios the concentration of the Au precursor was adjusted. For an Au/CdSe ratio of 1.3, 4.2 mg (20 μmol) of dodecanethiol and the Au(III)-stock solution containing 0.43 mg (1.4 μmol) of $AuCl_3$ and 0.68 mg (2.2 μmol) of DTAB were mixed with toluene to a total volume of 2.0 mL and shaken for 5 min (no sonication in order to prevent preliminary Au nucleation). After injecting the colorless solution, the reaction was left to stir at room temperature for 1 h.

CHARACTERIZATION

TEM Characterization. Standard transmission electron microscopy was carried out with a JEOL JEM 1011 microscope with a thermal emitter operated at an accelerating voltage of 100 kV. High resolution TEM micrographs at reduced temperature (96 K) were obtained with a JEOL JEM 2200FS (UHR) equipped with a field emitter as well as CESCOR and CETCOR correctors and a cryo sample holder. EDX data was recorded with a Philips CM 300 UT with an EDAX DX-4 system operated at 200 kV. Purified samples (10 μL) were drop-casted onto carbon covered copper grids. Medium values of nanoparticle dimensions were determined from at least 210 counts with Image-J software.

XPS Characterization. Samples of NPs and HNPs on HOPG were fixed with conductive carbon tape to the samples holders and inserted in a prevacuum chamber, prior to the XPS measurements. X-ray photoelectron spectroscopy has been performed at the "Helmholtz Zentrum Berlin für Materialien und Energie GmbH", BESSY II with different photon energies. No beam induced changes were detected in thin deposits of NPs prepared by drop-casting. All spectra were recorded at room temperature with a pass-energy of 20 eV. Binding energies were calibrated using the Csp^2 peak at 284.5 eV as reference.

DOI: 10.1021/acs.chemmater.6b00287
Chem. Mater. 2016, 28, 2704−2714

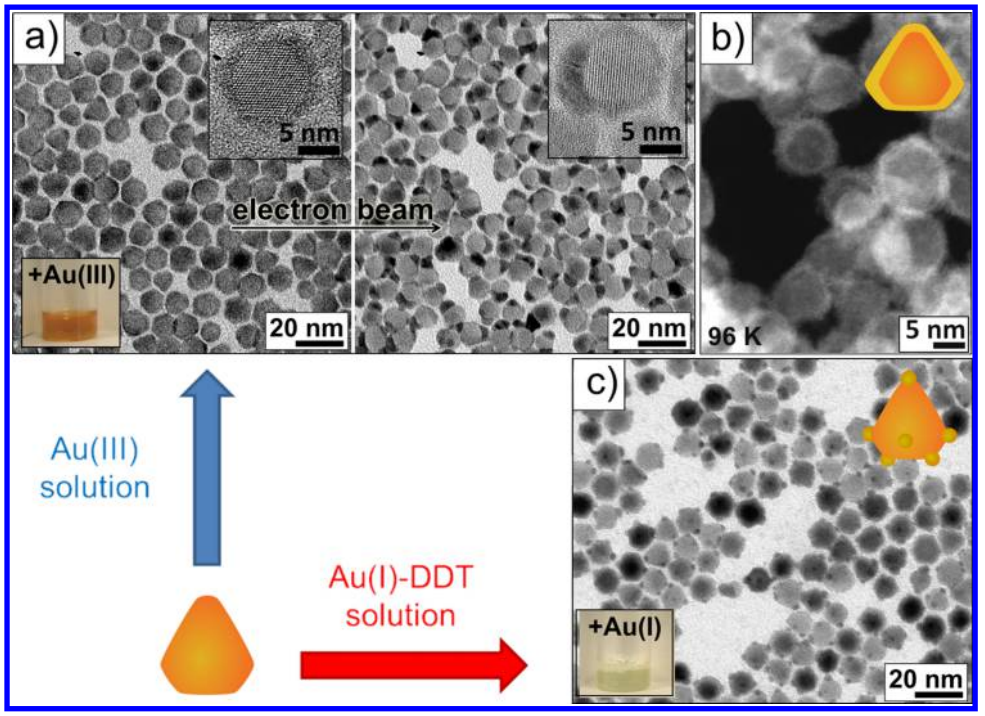

Figure 1. (a) TEM images of pyramidal CdSe NPs incubated with Au(III)-stock solution and taken immediately after focusing (Au/CdSe: 2.8). Within seconds to minutes, depending on the beam intensity and the amount of Au, the interaction with the electron beam induces migration of the Au atoms previously distributed over the surface of CdSe and its merging into Au clusters (200 kV acceleration voltage, 3 min between left and right). The insets show two representative particles at the corresponding stage. (b) At reduced temperature (96 K) the movement of the Au atoms is slowed down, which allows the visualization of the shell-like morphology of the Au deposits in STEM mode. (c) By adding Au(I)−DDT precursor spherical Au deposits are obtained (Au/CdSe: 1.4).

Experimental spectra were deconvoluted using the XPSPEAK 4.1 software with symmetric Gaussian−Lorentzian product functions to approximate the line shapes of the fitting components. In order to fit the Cd and Se signals in HNPs, the binding energy, width (fwhm), and % of Gaussian−Lorentzian of the initial CdSe NPs have been kept constant.

XRD Characterization. The NPs and HNPs were deposited onto a polished Si wafer by drop-casting. XRD measurements were carried out with a Philips X'Pert PRO MPD with Bragg- Brentano geometry and a Cu (Kα) X-ray source emitting at 0.154 nm. Backgrounds were subtracted with the X'Pert Highscore Plus software.

Mass Spectrometry. The samples were analyzed in a mass spectrometer with a QTOF hybrid analyzer, QSTAR pulsar i model (AB Sciex). Au precursor solutions were injected via direct infusion in an electrospray source with a flux rate of 20 μL/min, and the spectra were acquired in the positive and negative detection ion modes at the Sidl UAM Madrid.

Electrochemical Measurements. Voltammetric measurements were performed under N_2 atmosphere in a conventional three-electrode setup. A glassy-carbon bar as working electrode, a square sheet of platinum (99.998% purity) as counter electrode, and a homemade Ag/$AgNO_3$ as reference electrode (Ag/0.01 M $AgNO_3$// 0.1 M TBAP in acetonitrile) were used. All potentials are quoted with respect to the Ag/$AgNO_3$ reference electrode (E Ag/$AgNO_3$ ≈ 0.5326 V vs NHE). Tetrabutylammonium perclorate (TBAP) 0.1 M was used as supporting electrolyte in anhydrous acetonitrile. All electrochemical measurements were carried out under inert conditions obtaining a potential window of 4 V, corresponding to the stability of the solvent (acetonitrile). The experiments were performed in solutions thermostated at (25 ± 0.5) °C. The electrochemical experiments were performed with an Autolab PGSTAT20 (EcoChemie) with a GPES 4.9 software. The NPs and HNPs were adsorbed on the glassy-carbon electrode by drop-casting, while the Au precursor solutions were dissolved in the electrolyte solution.

MD Simulations. Simulations based on density functional theory (DFT) employ geometry optimization in order to evaluate the interaction/adsorption of molecules (ligands) on crystals. Such simulations represent the situation at 0 K. Most chemical reactions (also at surfaces) require an activation energy which can be provided by thermal energy. Thus, molecular dynamic simulations are necessary. In order to simulate the adsorption and possible decomposition of precursor molecules on nanoparticles, we employ molecular dynamics simulations within the DFT framework. For that, we used the versatile software package CP2K/QUICKSTEP[43] with the PADE LDA functional, the DZVP basis set, and a corresponding GTH-PADE potential. An individual wurtzite-CdSe nanocrystal with 123 Cd and 123 Se atoms and the respective ligand molecules are simulated with periodic boundary conditions where the box dimensions are sufficiently large to avoid interaction between virtual neighboring molecular structures. The atom positions of the CdSe nanocrystal were kept fixed using the corresponding experimental values (a = 0.430 nm, c = 0.702 nm), while the ligand molecules were free to move or decompose. The simulation temperature (NOSE thermostat, time constant 50 fs, NVT ensemble) was 300 K, as in the experiments.

All MD simulations ran for 20 ps, after which an additional geometry optimization has been performed at 0 K. In all cases the geometries before and after this optimization are similar, the main difference being shorter bonds between the adsorbed moieties and the CdSe surface atoms.

■ RESULTS AND DISCUSSION

We followed a seeded-growth approach based on a straight forward method applied to deposit Au on Cd chalcogenides NPs in organic solution.[6] $AuCl_3$ was solubilized with dodecyltrimethylammonium bromide (DTAB) in toluene forming an orange complex (named Au(III)-stock solution in the following).[27] To reduce Au(III) to Au(I) before deposition on the seed NPs, this complex is usually mixed with mild

DOI: 10.1021/acs.chemmater.6b00287
Chem. Mater. 2016, 28, 2704−2714

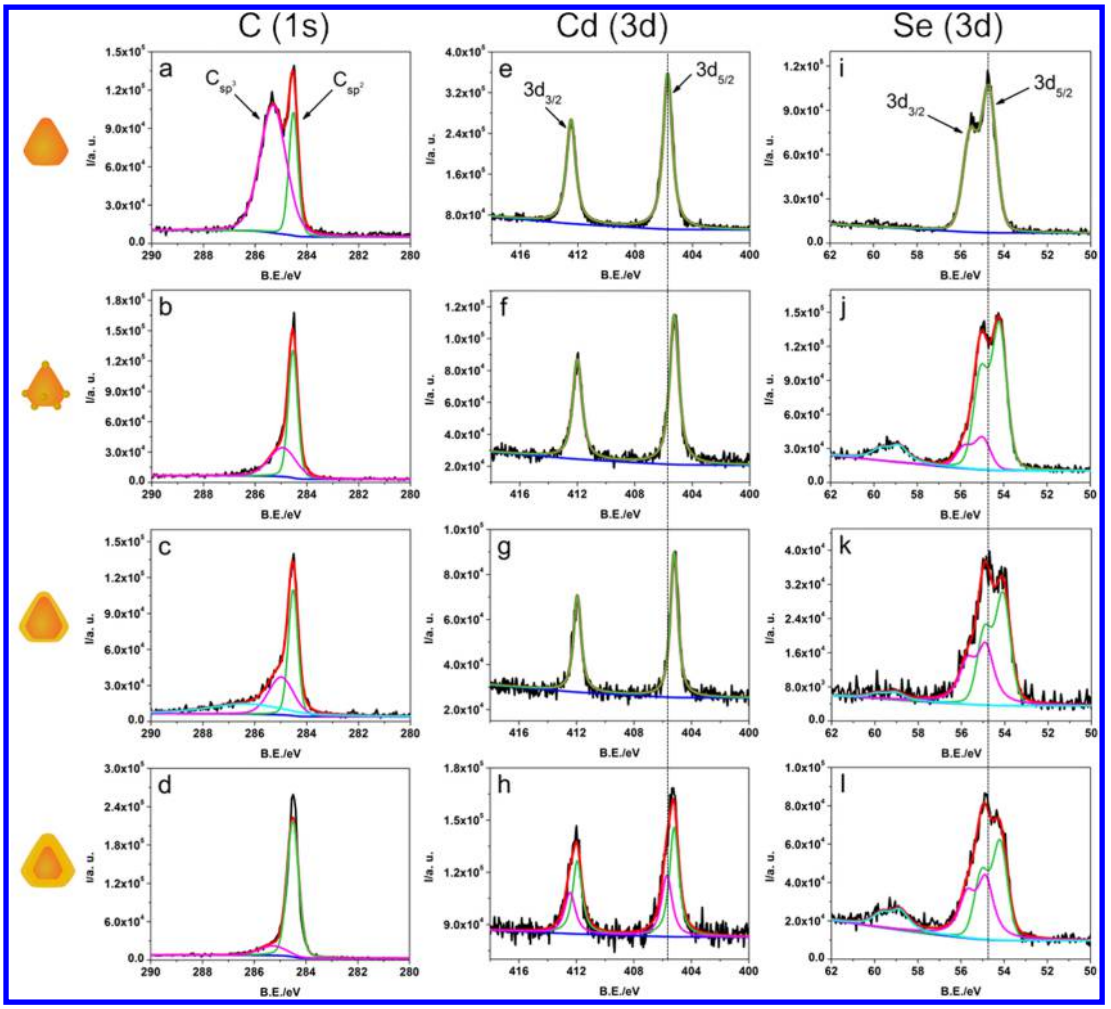

Figure 2. XPS spectral regions of C 1s, Cd 3d, and Se 3d for pure CdSe NPs (first row), CdSe NPs with spherical gold deposits (second row), and CdSe NPs covered with a thin gold shell (third row) and with a thicker Au shell (fourth row).

reducing agents such as amines or thiols.[28,29] In our case, an excess of dodecanethiol (DDT) has been added to the Au(III)-stock solution. Thiols reduce Au(III) to Au(I) very fast, evidenced by the fact that the solution turns colorless within 5 min (see Figure S1 in the Supporting Information). These two solutions, with different oxidation states (Au(III)-stock solution and Au(I)−DDT), were employed to examine their effect on the Au deposition onto CdSe pyramidal NPs.

The incubation of CdSe NPs in the Au(III)-stock solution results in the formation of a shell around the whole NP (Figure 1a,b). The thickness of the shell can be controlled by simply changing the concentration of the Au stock solution (see Experimental Methods). This shell is similar to that observed in an earlier study, where we reported the formation of a Au shell on hexagonal pyramidal CdSe NPs with Au-DTAB solutions containing amines.[17] Making this shell visible proved intricate, as it was readily destroyed by interaction with the electron beam in the TEM and lasted only for seconds after focusing. In Figure 1a the formation of metal deposits with a globular morphology on one or several sides of the seed NP produced by the effect of the beam exposure is shown. Such destructive interactions are known from Au NPs characterization where precursor complexes can be reduced from Au(III) to Au(I) or even Au clusters during inspection.[30] Both electron beams and heat (due to thermal stress) may induce structural rearrangements and even degeneration of the original structure in HNPs of CdSe-Au and CdS-Au. However, by reducing the temperature during inspection (96 K), atomic migration can be slowed down so that high resolution recordings and STEM micrographs of the shell can be obtained, as it is shown in Figure 1b.

On the contrary, the incubation of CdSe NPs with the Au(I)−DDT precursor solution leads to the formation of dot-shaped deposits. These deposits, that are stable during TEM inspection, are spherical and differ notably from those evolving from the Au-shell TEM inspection (Figure 1c). The size of the initial CdSe NPs is around 12 nm, and it is reduced to approximately 10 nm after the Au(III)-deposition process. In the case of the dot-like deposits, this reduction is only around 0.5 nm. We also observe a slight reduction in the Cd content of the samples upon Au deposition, ascertained by EDX analysis (Table SI in the Supporting Information). The EDX results show two opposing tendencies: the Cd (atomic %) content decreases whereas the Au (atomic %) content increases as the NPs are incubated with Au, leaving the Se content practically constant. Mechanistically, the final size of the resultant particle is determined by two competing processes, namely, the growth of the Au deposit in the form of dots or a shell and an etching of the CdSe NPs, an effect also observed previously.[9] This etching effect might be caused by bromide or chloride ions released from the precursor,[31] which would react with the Cd

DOI: 10.1021/acs.chemmater.6b00287
Chem. Mater. 2016, 28, 2704−2714

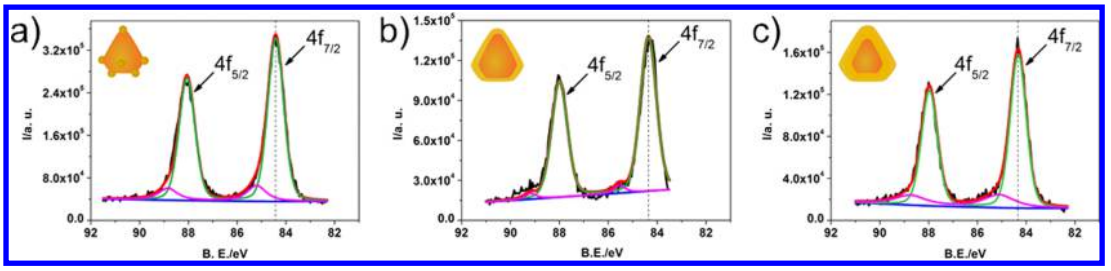

Figure 3. XPS spectra of Au 4f for CdSe NPs with spherical Au deposits (a) and CdSe NPs covered with a thin Au shell (b) and with a thicker Au shell (c).

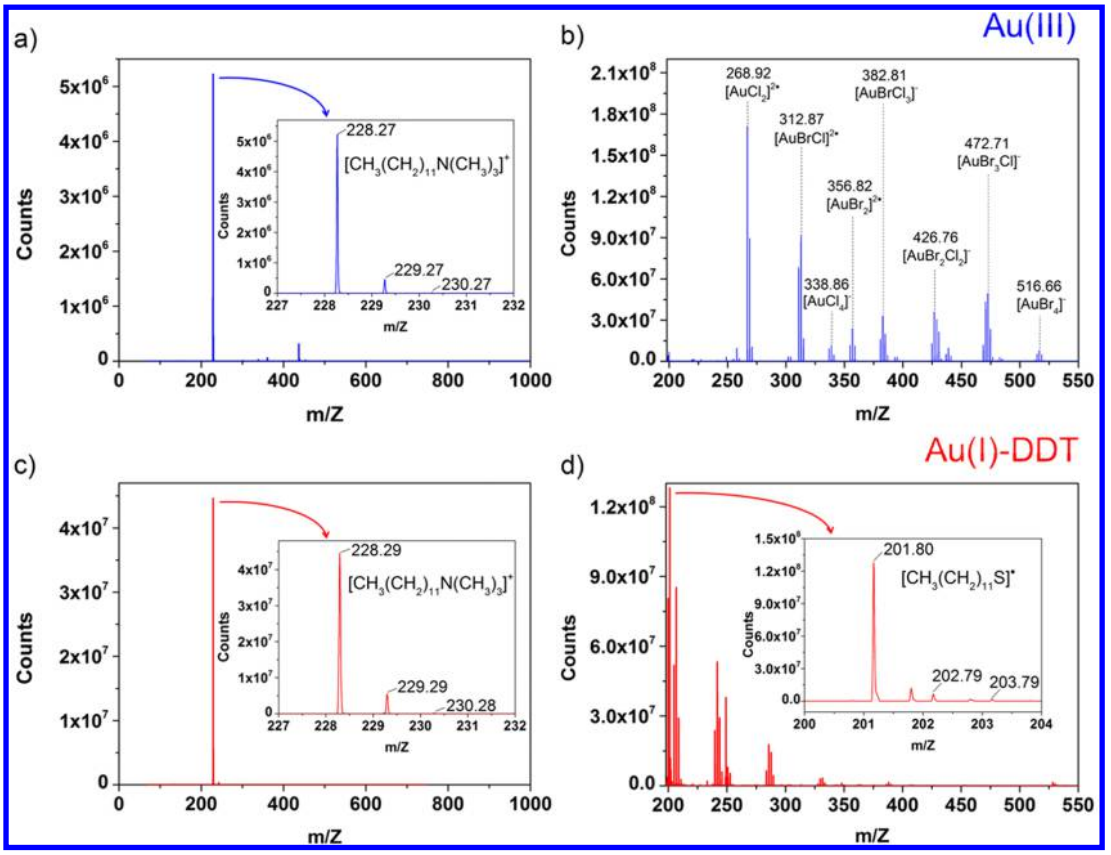

Figure 4. Mass spectra of the Au precursors used to form shell (Au(III)-stock solution, $AuCl_3$ + DTAB; up, blue) or dot-like deposits (Au(I)−DDT precursor solution, $AuCl_3$ + DTAB + DDT; down, red) on CdSe NPs. (a) and (c) correspond to the positive-ion mode and (b) and (d) to the negative-ion mode of the mass spectra.

surface atoms, leaving free Se sites behind to interact with the Au cations. This would explain why it is possible to obtain a core−shell-like heterostructure with pyramidal NPs and not with rod-shaped seeds. As mentioned earlier, the {101} planes of the wurtzite structure can be rich in one type of ion, which in the case of Se provides the prerequisite for binding of Au to a majority of the NP surface.

In order to account for differences in the CdSe NPs upon Au deposition, XPS analyses have been carried out. Figure 2 shows the XPS analysis (C 1s, Cd 3d, and Se 3d regions) performed on plain pyramidal CdSe NPs (first row), CdSe NPs exhibiting dot-shaped deposits (second row), and NPs with a thin (Au/CdSe: 2.0, see Experimental Methods) and a thick Au shell (Au/CdSe: 2.9) (third and fourth row, respectively).

As it can be seen, in all C 1s spectra (Figures 2a−d) there is one signal at 284.5 eV, corresponding to the Csp^2 contribution of the HOPG substrate, which has been used as a reference for binding energy calibration. For pure CdSe NPs (Figure 2a) the C 1s signal shows another well-defined contribution, centered at 285.3 eV, corresponding to the long alkyl chains of the initial ligands. This Csp^3 contribution decreases dramatically for every hybrid system regardless the morphology of the Au deposits (either dots or shell), indicating a partial or total displacement of phosphonic ligands upon Au growth.

The second column of Figure 2 shows the Cd 3d spectra (e-h): Two peaks can be observed in these spectra due to the spin−orbit splitting, Cd $3d_{5/2}$ and Cd $3d_{3/2}$, at 405.7 and 412.5 eV, respectively, related to Cd in CdSe. As it can be seen in spectra f, g, and h, the core Cd 3d signals are shifted to smaller binding energies (405.2 and 412.0 eV for the Cd $3d_{5/2}$ and Cd $3d_{3/2}$, respectively) upon Au growth. Similar effects have been observed in PbSe nanocrystal thin films upon ligand removal and have been attributed to the modification of the electronic density and, hence, of the local dielectric constant.[32] This interpretation is in good agreement with the elimination of the alkyl chains contribution evidenced by the C 1s core level

DOI: 10.1021/acs.chemmater.6b00287
Chem. Mater. 2016, 28, 2704−2714

Scheme 1. Reactions for Au(III)-Stock Solution (1) and Au(I)−DDT (2)

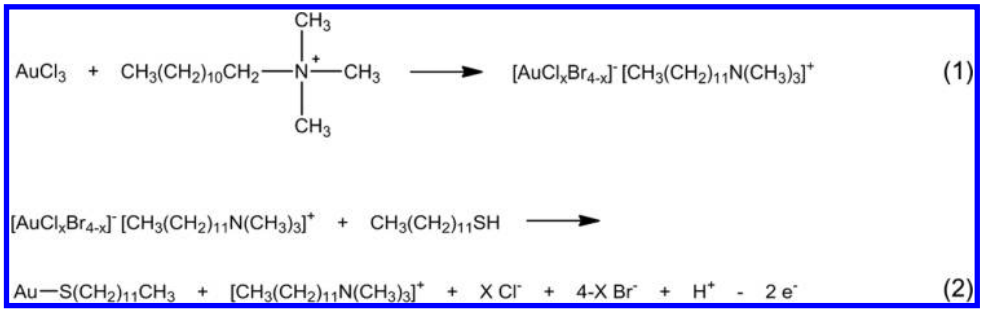

analysis. An alternative explanation could be the changes in the oxidation state (or in the chemical environments) of Cd and Se atoms,[19] due to the formation of Au−Se bonds. In the case of the HNPs with the thickest shell (2 h), the Cd 3d spectrum shows an additional oxidized component centered at higher binding energy (for a better display the comparison between the raw and fitted data is depicted in Figure S2 in the Supporting Information). Rather than considering this component as new, it is understood as a change in the electronic density due to unbounded Cd atoms. The absence of Cd oxidized components for CdSe covered by dotted Au (2f) and thin Au shell (2g) might be the result of sensitivity limitations.

In the third column of Figure 2 the spectra of the Se 3d peak are represented (i−l). This peak is also composed of two contributions (Se $3d_{5/2}$ and $3d_{3/2}$) due to the spin−orbit coupling. In the case of pyramidal CdSe NPs, the Se $3d_{5/2}$ is localized at 54.7 eV and is related to the Se^{2-} contribution of bulk CdSe.[33] Upon Au growth, two different changes in the Se peaks can be observed: The first one corresponds to a shift to lower binding energy values (from 54.7 to 54.2 eV), as previously described for the Cd signal and probably also related to the removal of ligands. The second change consists of the appearance of a new contribution at higher binding energy (54.9 eV) assigned to the oxidized Se sites involved in the Au(III) reduction to form Au−Se bonds. A similar Se binding energy (around 55.2 eV) assigned to covalent Au−Se bonds for Au NPs stabilized with alkaneselenate ligands has been previously recorded.[34] While the new Se contribution is visible for the three Au−CdSe hybrid systems at the same binding energy, higher intensity is recorded for NPs covered by a gold shell, indicating a higher oxidized surface in this case. Furthermore, an oxidized Se contribution appears at 58.8 eV in the spectra of every hybrid system resulting from unavoidable environmental oxidation during sample preparation and insertion in the XPS chamber.[35]

To account for differences in the Au deposits, Au 4f signals were also recorded and are shown in Figure 3. Au 4f signals are composed of two contributions, corresponding to the Au $4f_{7/2}$ and $4f_{5/2}$ energy levels at 84.4 and 88.0 eV, respectively. Interestingly, since the binding energy of metallic Au is 84.0 eV, our data indicates that Au deposits must not be in elemental form but in a higher oxidation state, such as that reported for Au−Se bonds.[34] Furthermore, as it can be seen in Figure 3, for all CdSe-Au HNPs an extra component at higher binding energies is observed. This small contribution has a binding energy of 84.9 eV for the CdSe NPs decorated with Au dots and 85.5 and 85.1 eV for the NPs covered with a thinner and thicker Au shell, respectively. Rather than assigning these higher binding energy components to an extra higher oxidation state of Au, this component is understood as the contributions of Au surface atoms with different environments. The presence of a Au−Se bond (and not metallic Au(0)) is also supported by the X-ray diffractograms shown in Figure S3 in the Supporting Information.

Thus, if the final composition of the Au deposits is similar regardless the oxidation state of the precursor, the question that arises is why they grow as dots or as a shell. Despite the common notion that DDT reduces Au(III) in halide complexes, we aimed to obtain a detailed characterization of the two gold precursor solutions. To this aim we have performed mass analysis and cyclic voltammetry. Figure 4a,b corresponds to the positive and negative ion parts of the mass spectra of the complex formed from $AuCl_3$ and DTAB (Au(III)-stock solution) and Figure 4c,d to those of the compound formed by adding DDT to this complex (Au(I)−DDT). The m/z values can be also found in Table SII in the Supporting Information. The mass analysis of the positive-ion mode of the spectra (Figure 4a,c) exhibits a similar and intense peak at m/z: 228.2, which can be assigned to the alkylammonium cation ($[CH_3(CH_2)_{11}N(CH_3)_3]^+$) in both complexes. However, very different spectra are acquired in the negative-ion mode. In Figure 4b the molecular ion peaks of every possible combination of Au with halides complexes ($AuCl_xBr_{4-x}^-$) is evidenced, confirming that the oxidation state of Au is Au(III) (see peak details in Table SII in the Supporting Information). After addition of DDT (Figure 4d), the molecular ion peaks related to the $[AuCl_xBr_{4-x}]^-$ complexes are not detected, and a new peak corresponding to the radical breakup of DDT at m/z: 201.1 can be found (Supporting Information, Table SII). This result points to the reduction of Au(III) to Au(I) in which the thiol group of the DDT acts as reducing agent. Thus, the MS results support that the oxidation state of the Au precursors differs. According to these MS results we propose the following reactions to form the Au(III)-stock solution (**1**) and Au(I)−DDT precursor solution (**2**), according to Scheme 1.

In order to further verify the different oxidation states of the Au precursors and test their electrochemical response, cyclic voltammetry (CV) was applied. Figure 5a,b shows the obtained voltammograms of the pure Au(III)-stock solution and the Au(I)−DDT precursor solution, respectively. For the former (Figure 5a), the first reduction peak at −0.1 V corresponds to the Au(III) to Au(I) reduction process and the second reduction peak at −1.1 V corresponds to Au(0) metallic deposit formed by the reduction of Au(I) to Au(0). Scanning further, the oxidation of halides (Cl^- and Br^-) over the Au metallic deposit (peaks at 0.3 and 0.9 V) and over the glassy-carbon electrode at more anodic potentials (around 1.1 V) can be clearly identified.[36−40] However, in the voltammogram

DOI: 10.1021/acs.chemmater.6b00287
Chem. Mater. 2016, 28, 2704−2714

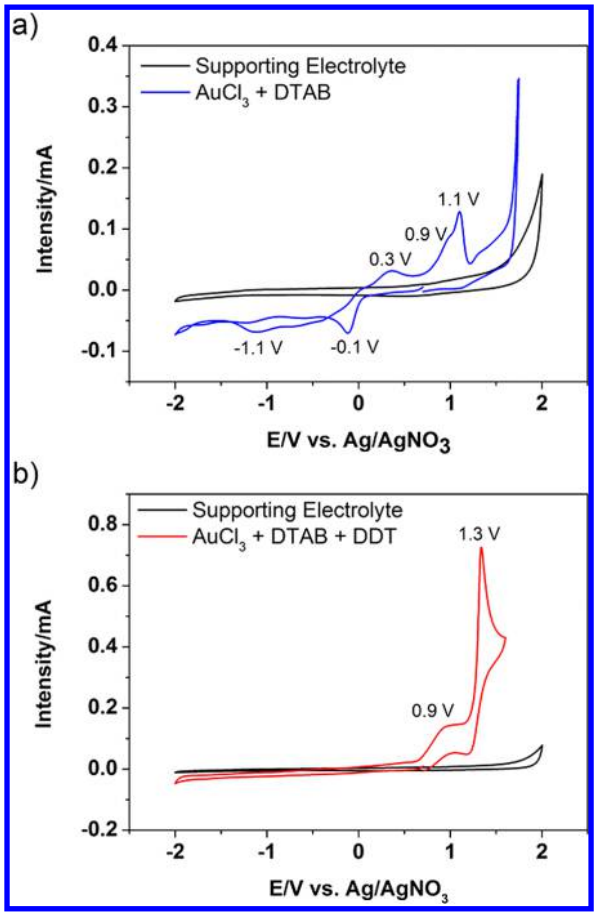

Figure 5. Cyclic voltammograms of (a) Au(III)-stock solution ($AuCl_3$ and DTAB) and (b) Au(I) solution formed by adding DDT to the previous Au(III)-stock solution. Electrolyte solution: 0.1 M TBAP in acetonitrile; ν = 0.1 V s^{-1}.

obtained with the precursor solution used to grow dots, Au(I)−DDT (Figure 5b), no reduction process can be recorded, which supports the absence of Au(III) and the high stability of the Au−S bond in the compound (no reduction of Au(I) to Au(0) is recorded).

In order to evaluate differences in the Au−CdSe HNPs with dots or shell, they have also been characterized by CV and compared with both pure CdSe and pure Au NPs (prepared from the Au(III) stock solution by reduction with tetrabutylammonium borohydride). Figure 6 shows the voltammograms of pyramidal CdSe NPs (a), NPs with Au−Se dot-like deposits (b), with a thin Au−Se shell deposit (c) and the voltammogram of pure Au dots (d). For the plain CdSe pyramidal NPs, a first cathodic scan does not show any charge transfer process (data not shown). This is in good agreement to our previous results which showed that the cathodic response in the voltammogram is exclusively related to the reduction of previously oxidized species.[35] However, the anodic part of the voltammogram exhibits two well-defined peaks at 1.2 and 1.5 V, which correspond to the Se oxidation and might be related to different atomic chemical environments or Se atoms located in different NPs facets.[35] When Au is added to the CdSe seed NPs, regardless the morphology of Au deposits, the oxidation onset is shifted from 1.0 V to less anodic potentials (to ∼0.6 V, blue arrow in Figure 6b,c) with respect to bare CdSe NPs (blue arrow in Figure 6a). In the voltammogram of Au NPs (Figure 6d) we can observe the oxidation of Au at those potentials

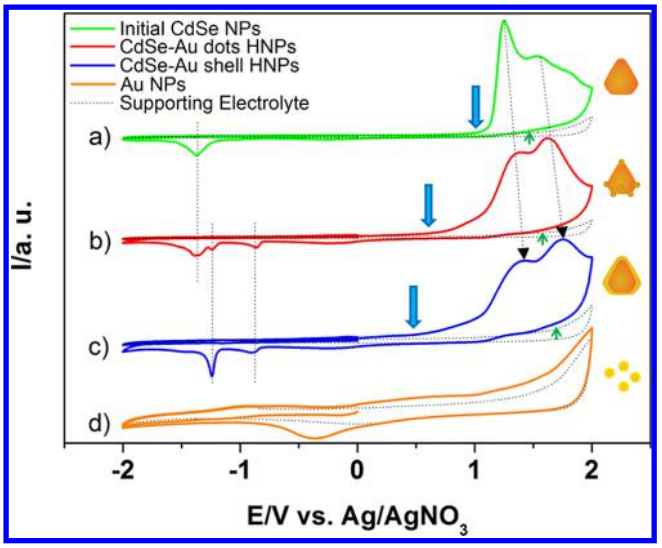

Figure 6. Cyclic voltammograms of seed pyramidal CdSe NPs (a), CdSe HNPs decorated with dot-like deposits on the vertices of the pyramids (b), CdSe HNPs covered by a shell deposit (c), and Au NPs (d) deposited on a glassy carbon electrode. Electrolyte solution: 0.1 M TBAP in acetonitrile; ν = 0.1 V s^{-1}. Dotted black arrows mark the shifts in the oxidation peaks. Blue arrows point out the differences in the oxidation onset. Green arrows designate the Se oxidation current obtained during the cathodic scan.

(∼0.6 V). Thus, the shift of the oxidation onset for the HNPs may be due to Au oxidation. We can also observe that the peaks attributed to the Se oxidation (initially at 1.2 and 1.5 V) are shifted to more anodic potentials for every HNPs system (see dotted arrows from part a to part c of Figure 6). This fact is only the consequence of the higher overpotential required to oxidize Se in the presence of Au. Interestingly, the oxidation charges for the HNPs are lower than the oxidation charge of CdSe NPs in the absence of Au. The voltammetric charge is 5356.12 μC for the pure CdSe seed NPs, 4423.47 μC for the CdSe NPs with deposited Au dot, and 3535.71 μC for CdSe NPs covered by an Au shell, which means that the charge decreases by 17% for the HNPs with Au−Se dots and by 34% for the HNPs with a Au−Se shell. Since all voltammograms were recorded for the same NP concentration, the oxidation charges can be directly compared. Curiously enough, in the Se 3d spectra previously shown (Figure 2j,k), the area corresponding to the oxidized Se_{Au-Se} component in the HNPs with Au−Se dots and Au−Se thin shell is 18% and 40% of the total Se area of that of the HNPs, respectively. These values are in good agreement with the decrease of charge in the corresponding voltammograms mentioned previously. This indicates that during an anodic scan only those Se atoms bonded to Cd can be oxidized, since Se in the Au−Se deposits is already oxidized. In fact, if the Au−Se was oxidized during the anodic scan, the total voltammetric charge of CdSe NPs covered by a thin Au−Se shell would increase compared to CdSe NPs with Au−Se dots and the latter compared to the bare CdSe NPs. On the other hand, it must be taken into account that Au atoms of the deposits are susceptible to be oxidized. If that would be the case, the oxidation charge should increase with increasing Au concentration from pure CdSe NPs, to HNPs covered with dots or shell deposits, in contrast to the obtained results. For these reasons it can be concluded that Au atoms in Au−Se deposits are very stable, i.e., are not oxidized in the applied potential range, and only unbounded Au

DOI: 10.1021/acs.chemmater.6b00287
Chem. Mater. 2016, 28, 2704−2714

could be oxidized, its charge contribution being negligible as indicated by the reduction charge.

In the cathodic scan from +2 V to the negative direction, an oxidation current (indicated with green arrows in Figure 6) was observed at anodic potentials around 1.5 V. In HNPs this current is the balance of two different redox processes that take place simultaneously, namely, the oxidation of Se of CdSe NPs and the partial reduction of Au (Au oxides) at the expense of the Se oxidation. This process produces a shift to less cathodic potentials for the reduction of Au oxides, as confirmed in Figure S4 (see Supporting Information). Notably there is no evidence of adsorption/desorption of thiols in the cathodic scan of HNPs which is further supported by the voltammogram of Au dots in which we only observed the reduction of Au oxides (Figure 6d).[41]

For negative potentials, both pure CdSe NPs and HNPs show a reduction peak centered at −1.37 V whose intensity decreases from pure CdSe NPs to HNPs with Au−Se dots and practically vanishes for HNPs with an Au−Se shell. This peak can be attributed to the simple reduction of oxidized Se species formed in the previous anodic scan. Moreover, an extra reduction peak at −1.2 V appears for HNPs whose contribution becomes higher as the amount of Au increases (from dots to shell deposits). To understand the presence of this peak, the reduction of the Au(III)-stock solution shown in Figure 5a should be taken into account. As previously shown, the reduction takes place in different steps. First Au(III) is reduced to Au(I) and finally to Au(0) in a further step. The reduction peak at −1.1 V corresponds to the mass deposit formed by the reduction of Au(I) to Au(0). These results suggest that the reduction peak at −1.2 V might be related to the reduction of Au(I) atoms that are not bonded to Se.

Gathering the characterization of the precursors and the CdSe HNPs by means of XPS, MS, and electrochemistry it is clear that the different morphologies of the deposits are related to the different oxidation states of the Au precursor. However, the surface composition of the NP may also play a role, not only driving the final morphology of the deposits but also their final oxidation state. In the literature, the very first step of the deposition process of the metal on the NP surface is a matter of discussion. Some authors argue that crystalline metal domains form after precursor molecules adsorb on the surface and are reduced by anions on the seed.[9,42] Others assume an attachment and growth of metal clusters formed in solution by reduction with added amines or other mild reducing agents.[1,3] In order to understand the possible deposition mechanism and the formation of dots or a shell, molecular dynamics simulations were carried out. The simulations have been performed considering (i) a noncapped CdSe NPs surface and (ii) CdSe with preadsorbed Cl on the surface, to simulate a closest scenario of the pyramidal NPs surface, according to our previous works.[25,26] Figure 7 shows the simulations for CdSe NPs incubated with the Au(III)-stock solution, whose ionic form corresponds to the complex $[AuCl_xBr_{4-x}]^-$ $[CH_3(CH_2)_{11}N(CH_3)_3]^+$. Figure 7a,b correspond to the plain noncapped CdSe NPs and Figure 7c,d to CdSe NPs capped with Cl. For charge and spin neutrality two Cl atoms on opposite sides of the NP have been simulated, although only one is visible in the images. The simulations show several differences. In the case of noncapped NPs the Cl atom of the complex interacts first electrostatically with the surface (Figure 7a, after 1 ps). We hypothesize that this first interaction (involving Cl and Br anions reacting with the surface) may

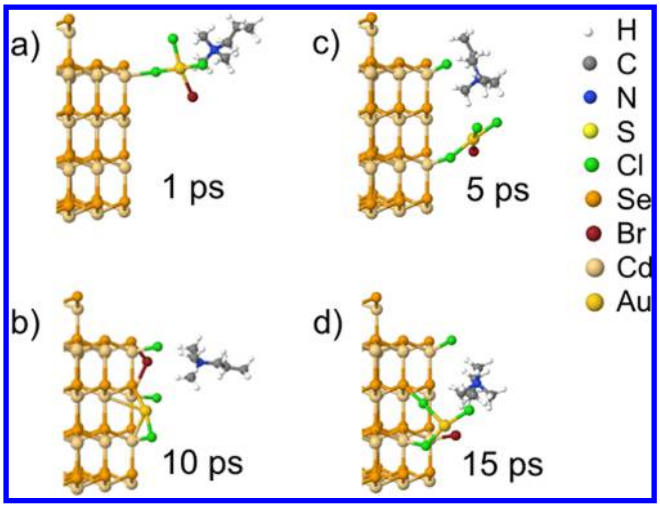

Figure 7. Molecular dynamic simulations of noncapped CdSe NPs (a, b) and Cl-capped CdSe (c, d) incubated with Au(III)-stock solution at 300 K.

cause the release of surface atoms, which would explain the decrease in the Cd content (proven by EDX) and the related etching effect (see Figure 1). After 10 ps (Figure 7b) the complex fully decomposes, releasing the alkylammonium cation ($[CH_3(CH_2)_{11}N(CH_3)_3]^+$). At the same time, Au gets adsorbed on the NP surface, and the initial Au(III) is reduced at the expense of Se^{2-}. The picture differs substantially when CdSe NPs are capped with Cl anions (Figure 7c,d): in this case, the electrostatic repulsion of the complex approaching the Cl-capped surface slows down the interaction with the CdSe surface, hindering the decomposition of the complex at a similar time. For this reason Figure 7c,d depicts the molecular dynamics after 5 and 15 ps, respectively, where the final configuration shows Au interacting with the NP surface mediated by Cl atoms from the complex. Although a simplification, this simulation confirms that the reduction of the Au precursor on the NP surface takes place in a different way depending on the surface constitution. For noncapped CdSe NCs, further Au(0) would nucleate on the Au−Se interface, while in the case of Cl-capped CdSe NCs, the first interaction is mediated by Cl and further nucleation (not shown) follows a similar behavior, where Cl is always involved in the reaction between Au and Se surface atoms. This result is in good agreement with the formation of a Au−Se compound with a possible SeClAu composition.

To explain the formation of dots, the simulation was performed with $AuS(CH_2)_2CH_3$ as precursor solution instead of the longer DDT, to reduce the simulation time (Figure 8). After 1 ps the simulations show that for noncapped CdSe NPs (Figure 8a,b) Au interacts first with Se. In contrast, for NPs capped with Cl (Figure 8c,d), the Au(I) precursor interacts with that Cl. In both cases, the interaction takes place with atoms on the vertices, contrary to the preceding case where those sites were not favorable for the complex. After 10 ps (Figure 8d), the final configurations show that for Cl-capped NPs Cl is involved in the interaction between the Au(I) precursor and the surface. In both cases the Au(I) precursor does not decompose but gets absorbed on the NP surface. As previously mentioned, in this case the CdSe NPs also reduce their initial size. This etching effect might be related in this case to halogens and/or halides free in solution produced as byproducts when the Au(III)-stock solution is reduced to Au(I)

DOI: 10.1021/acs.chemmater.6b00287
Chem. Mater. 2016, 28, 2704−2714

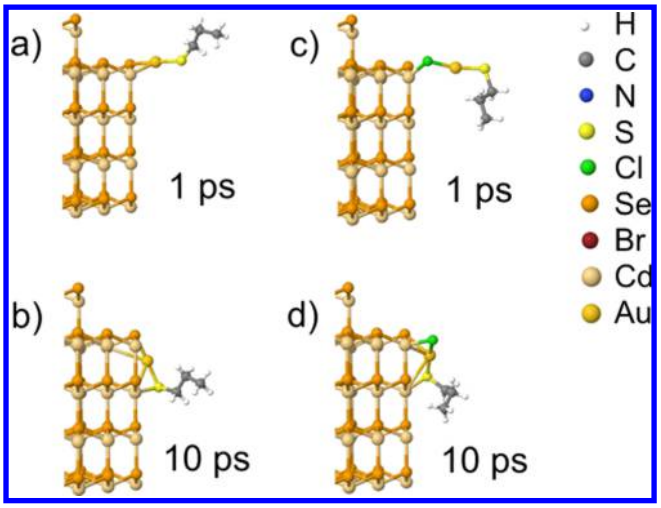

Figure 8. Molecular dynamic simulations of noncapped CdSe NPs (a, b) and Cl-capped CdSe (c, d) incubated with Au(I)−DDT precursor solution at 300 K.

by the presence of the thiol (DDT) (see eq 2 in Scheme 1). As in the former case, these different interactions may account for the absence of elemental Au on the surface of pyramidal CdSe capped with chloride anions, as confirmed by XPS.

Assuming the limitations of the simulations, which are performed considering perfect and stoichiometric crystals in vacuum, these results along with the HRTEM, XPS, and CV characterizations provide an accurate picture of the deposition process as well as a comprehensive understanding of the final composition and morphology of the deposits. We believe that this type of study is necessary to correlate potential synergetic properties (for example, conductivity or reactivity) obtained from the combination of materials in hybrid structures.

CONCLUSIONS

In this work, metal−semiconductor hybrid nanoparticle HNPs containing Au and CdSe were characterized by HRTEM (including low temperature STEM), XPS, MS, cyclic voltammetry, and molecular dynamics simulations. Differences in the reactivity of the distinct Au oxidation states of Au precursor solutions induce preferential deposition of dot-like deposits on the vertices of the CdSe seeds or a shell covering the whole NP surface. Evidenced by XPS and supported by molecular dynamics simulations, the Au deposits are not elemental, but most probably AuSe or AuSeCl. Such a composition may explain the instability of deposited Au shells and their transformation into dot-shaped deposits under the e-beam. The incomplete reduction of Au is driven by the surface chemistry of the CdSe seeds, which is composed of both phosphonic acids and chloride ligands. The results show that the deposition mechanism as well as the final morphology and composition of the deposits depend on two important factors: (i) the oxidation state of the Au precursor and (ii) the surface ligand composition. Both are essential issues to address in order to understand the deposition process and the key factors determining the evolving interface and related properties in a heterodeposition process. Such knowledge is not only valuable in regard to the formation and stability of hybrid nanostructures but also with respect to the fabrication of other heterostructures applied, for example, in catalytic processes.

ASSOCIATED CONTENT

Supporting Information

The Supporting Information is available free of charge on the ACS Publications website at DOI: 10.1021/acs.chemmater.6b00287.

Figure S1 with optical images of Au precursor solutions. Table SI with EDX analysis of CdSe NPs after Au deposition demonstrating the etching effect upon Au-deposition. Figure S2 with comparison between the raw and fitted data for spectrum Figure 2h. Figure S3 with XRD information on plain CdSe and HNPs with the thickest shell deposits, compared with wurtzite CdSe, AuSe, and Au. Figure S4 with voltammograms of reduced Au oxides. Table SII with the parameters of the peaks found in the negative-ion mode of the Au precursor solutions by MS spectrometry (PDF)

AUTHOR INFORMATION

Corresponding Authors

*C. Klinke. E-mail: klinke@chemie.uni-hamburg.de.

*B.H. Juarez. E-mail: beatriz.hernandez@imdea.org.

Present Address

[▽](M. Meyns) Catalonia Institute for Energy Research (IREC), Jardins de les Dones de Negre, 1 2[a]Pl, Sant Adria de Besòs 08930, Barcelona, Spain.

Author Contributions

[¶](L. de la Cueva and M. Meyns) These authors contributed equally.

Notes

The authors declare no competing financial interest.

ACKNOWLEDGMENTS

C.K. and M.M. acknowledge the European Union for the ERC Starting Grant 2D-SYNETRA (304980, Seventh Framework Program FP7) and the Deutsche Forschungsgemeinschaft for granting the project KL 1453/9-1. We thank Andreas Kornowski for high resolution TEM micrographs at room temperature and under cryogenic conditions, EDX data, and helpful discussions. We thank M[a] Jesús Vicente Arana for her help with the MS spectrometry analysis. B.H.J. is thankful for funding in the frame of the following projects: S2013/MIT-2740 from Comunidad de Madrid and FIS2012-33011 and MAT2013-47395-C4-3-R and FIS2015-67367-C2-1-P from the Spanish Ministry of Economy and Competitiveness. R.O. is thankful for FIS2012-33011. Furthermore, the authors thank the Helmholtz Zentrum Berlin to have benn granted access to the BESSY-II facility, in particular the SurICat UHV XPS station. N.G.B. acknowledges financial support by MINECO through the Ramon y Cajal program (RYC-2012- 10991) and by the European Commission Seventh Framework Programme (FP7) through the Marie Curie Career Integration Grant (322153-MINE).

REFERENCES

(1) Zeng, J.; Huang, J.; Liu, C.; Wu, C. H.; Lin, Y.; Wang, X.; Zhang, S.; Hou, J.; Xia, Y. Gold-Based Hybrid Nanocrystals Through Heterogeneous Nucleation and Growth. *Adv. Mater.* **2010**, *22*, 1936−1940.

(2) Costi, R.; Saunders, A. E.; Banin, U. Colloidal Hybrid Nanostructures: A New Type of Functional Materials. *Angew. Chem., Int. Ed.* **2010**, *49*, 4878−4897.

DOI: 10.1021/acs.chemmater.6b00287
Chem. Mater. 2016, 28, 2704−2714

(3) Carbone, L.; Cozzoli, P. D. Colloidal heterostructured nanocrystals: Synthesis and growth mechanisms. *Nano Today* **2010**, *5*, 449−493.
(4) Banin, U.; Ben-Shahar, Y.; Vinokurov, K. Hybrid Semiconductor−Metal Nanoparticles: From Architecture to Function. *Chem. Mater.* **2014**, *26*, 97−110.
(5) Salant, A.; Amitay-Sadovsky, E.; Banin, U. Directed Self-Assembly of Gold-Tipped CdSe Nanorods. *J. Am. Chem. Soc.* **2006**, *128*, 10006−10007.
(6) Mokari, T.; Rothenberg, E.; Popov, I.; Costi, R.; Banin, U. Selective Growth of Metal Tips onto Semiconductor Quantum Rods and Tetrapods. *Science* **2004**, *304*, 1787−1790.
(7) Meyns, M.; Willing, S.; Lehmann, H.; Klinke, C. Metal Domain Size Dependent Electrical Transport in Pt-CdSe Hybrid Nanoparticle Monolayers. *ACS Nano* **2015**, *9* (6), 6077−6087.
(8) Vaneski, A.; Susha, A. S.; Rodríguez-Fernández, J.; Berr, M.; Jäckel, F.; Feldmann, J.; Rogach, A. L. Hybrid Colloidal Heterostructures of Anisotropic Semiconductor Nanocrystals Decorated with Noble Metals: Synthesis and Function. *Adv. Funct. Mater.* **2011**, *21*, 1547−1556.
(9) Costi, R.; Saunders, A. E.; Elmalem, E.; Salant, A.; Banin, U. Visible Light-Induced Charge Retention and Photocatalysis with Hybrid CdSe-Au Nanodumbbells. *Nano Lett.* **2008**, *8* (2), 637−641.
(10) Schweinberger, F.; Berr, M. J.; Döblinger, M.; Wolff, C.; Sanwald, K. E.; Crampton, A. S.; Ridge, C. J.; Jäckel, F.; Feldmann, J.; Tschurl, M.; Heiz, U. Cluster Size Effects in the Photocatalytic Hydrogen Evolution Reaction. *J. Am. Chem. Soc.* **2013**, *135*, 13262−13265.
(11) Costi, R.; Cohen, G.; Salant, A.; Rabani, E.; Banin, U. Electrostatic Force Microscopy Study of Single Au-CdSe Hybrid Nanodumbbells: Evidence for Light-Induced Charge Separation. *Nano Lett.* **2009**, *9* (5), 2031−2039.
(12) Amirav, L.; Alivisatos, A. P. Photocatalytic Hydrogen Production with Tunable Nanorod Heterostructures. *J. Phys. Chem. Lett.* **2010**, *1*, 1051−1054.
(13) Berr, M. J.; Schweinberger, F. F.; Döblinger, M.; Sanwald, K. E.; Wolff, C.; Breimeier, J.; Crampton, A. S.; Ridge, C. J.; Tschurl, M.; Heiz, U.; Jäckel, F.; Feldmann, J. Size-Selected Subnanometer Cluster Catalysts on Semiconductor Nanocrystal Films for Atomic Scale Insight into Photocatalysis. *Nano Lett.* **2012**, *12*, 5903−5906.
(14) Naskar, S.; Schlosser, A.; Miethe, J. F.; Steinbach, F.; Feldhoff, A.; Bigall, N. C. Site-Selective Noble Metal Growth on CdSe Nanoplatelets. *Chem. Mater.* **2015**, *27*, 3159−3166.
(15) Saunders, A. E.; Popov, I.; Banin, U. Synthesis of Hybrid CdS-Au Colloidal Nanostructures. *J. Phys. Chem. B* **2006**, *110*, 25421−25429.
(16) Carbone, L.; Kudera, S.; Giannini, C.; Ciccarella, G.; Cingolani, R.; Cozzoli, P. D.; Manna, L. Selective reactions on the tips of colloidal semiconductor nanorods. *J. Mater. Chem.* **2006**, *16*, 3952−3956.
(17) Meyns, M.; Bastus, N. G.; Cai, Y.; Kornowski, A.; Juárez, B. H.; Weller, H.; Klinke, C. Growth and reductive transformation of a gold shell around pyramidal cadmium selenide nanocrystals. *J. Mater. Chem.* **2010**, *20*, 10602−10605.
(18) Jen-La Plante, I.; Habas, S. E.; Yuhas, B. D.; Gargas, D. J.; Mokari, T. Interfacing Metal Nanoparticles with Semiconductor Nanowires. *Chem. Mater.* **2009**, *21*, 3662−3667.
(19) Sheldon, M. T.; Trudeau, P.-E.; Mokari, T.; Wang, L.-W.; Alivisatos, A. P. Enhanced Semiconductor Nanocrystal Conductance via Solution Grown Contacts. *Nano Lett.* **2009**, *9* (11), 3676−3682.
(20) Mokari, T.; Sztrum, C. G.; Salant, A.; Rabani, E.; Banin, U. Formation of asymmetric one-sided metal-tipped semiconductor nanocrystal dots and rods. *Nat. Mater.* **2005**, *4*, 855−863.
(21) Juárez, B. H.; Meyns, M.; Chanaewa, A.; Cai, Y.; Klinke, C.; Weller, H. Carbon Supported CdSe Nanocrystals. *J. Am. Chem. Soc.* **2008**, *130*, 15282−15284.
(22) Juárez, B. H.; Klinke, C.; Kornowski, A.; Weller, H. Quantum Dot Attachment and Morphology Control by Carbon Nanotubes. *Nano Lett.* **2007**, *7* (12), 3564−3568.
(23) Hungría, A. B.; Juárez, B. H.; Klinke, C.; Weller, H.; Midgley, P. A. 3-D Characterization of CdSe Nanoparticles Attached to Carbon Nanotubes. *Nano Res.* **2008**, *1*, 89−97.
(24) Meyns, M.; Iacono, F.; Palencia, C.; Geweke, J.; Coderch, M. D.; Fittschen, U. E. A.; Gallego, J. M.; Otero, R.; Juárez, B. H.; Klinke, C. Shape Evolution of CdSe Nanoparticles Controlled by Halogen Compounds. *Chem. Mater.* **2014**, *26*, 1813−1821.
(25) Iacono, F.; Palencia, C.; de la Cueva, L.; Meyns, M.; Terracciano, L.; Vollmer, A.; de la Mata, M. J.; Klinke, C.; Gallego, J. M.; Juárez, B. H.; Otero, R. Interfacing Quantum Dots and Graphitic Surfaces with Chlorine Atomic Ligands. *ACS Nano* **2013**, *7* (3), 2559−2565.
(26) Palencia, C.; Lauwaet, K.; de la Cueva, L.; Acebrón, M.; Conde, J. J.; Meyns, M.; Klinke, C.; Gallego, J. M.; Otero, R.; Juárez, B. H. Cl-capped CdSe nanocrystals via in situ generation of chloride anions. *Nanoscale* **2014**, *6*, 6812−6818.
(27) Puddephatt, R. *The Chemistry of Gold*; Elsevier: Amsterdam, 1978.
(28) Yang, J.; Ying, Y. A general phase-transfer protocol for metal ions and its application in nanocrystals synthesis. *Nat. Mater.* **2009**, *8*, 683−689.
(29) Huo, Z.; Tsung, C.-K.; Huang, W.; Zhang, X.; Yang, P. Sub-Two Nanometer Single Crystal Au Nanowires. *Nano Lett.* **2008**, *8* (7), 2041−2044.
(30) Goulet, J. G.; Leonardi, A.; Lennox, R. B. Oxidation of Gold Nnoparticles by Au(III) Complexes in Toluene. *J. Phys. Chem. C* **2012**, *116*, 14096−14102.
(31) Lim, S. J.; Kim, W.; Jung, S.; Seo, J.; Shin, S. K. Anisotropic Etching of Semiconductor Nanocrystals. *Chem. Mater.* **2011**, *23*, 5029−5036.
(32) Rosen, L.; Sawvel, A. M.; Milliron, D. J.; Helms, B. A. Influence of Surface Composition on Electronic Transport through Naked Nanocrystal Networks. *Chem. Mater.* **2014**, *26*, 2214−2217.
(33) Shenasa, M.; Sainkar, S.; Lichtman, D. XPS Study of Some Selected Selenium Compounds. *J. Electron Spectrosc. Relat. Phenom.* **1986**, *40*, 329−337.
(34) Yee, C. K.; Ulman, A.; Ruiz, J. D.; Parikh, A.; White, H.; Rafailovich, M. Alkyl Selenide- and Alkyl Thiolate-Functionalized Gold Nanoparticles: Chain Packing and Bond Nature. *Langmuir* **2003**, *19*, 9450−9458.
(35) de la Cueva, L.; Lauwaet, K.; Otero, R.; Gallego, J. M.; Alonso, C.; Juárez, B. H. Effect of Chloride Ligands on CdSe Nanocrystals by Cyclic Voltammetry and X-ray Photoelectron Spectroscopy. *J. Phys. Chem. C* **2014**, *118*, 4998−5004.
(36) Aldous, L.; Silvester, D.; Villagrán, C.; Pitner, W. R.; Compton, R. G.; Lagunas, M. C.; Hardacre, C. Electrochemical studies of gold and chloride in ionic liquids. *New J. Chem.* **2006**, *30*, 1576−1583.
(37) Ongaro, M.; Gambirasi, A.; Favaro, M.; Kuhn, A.; Ugo, P. Asymmetrical modification of carbon microfibers by bipolar electrochemistry in acetonitrile. *Electrochim. Acta* **2014**, *116*, 421−428.
(38) Koelle, U.; Laguna, A. Electrochemistry of Au-complexes. *Inorg. Chim. Acta* **1999**, *290*, 44−50.
(39) Villagrán, C.; Banks, C. E.; Hardacre, C.; Compton, R. G. Electroanalytical Determination of Trace Chloride in Room-Temperature Ionic Liquids. *Anal. Chem.* **2004**, *76* (7), 1998−2003.
(40) Monzón, L. M. A.; Byrne, F.; Coey, J. M. D. Gold electrodeposition in organic media. *J. Electroanal. Chem.* **2011**, *657*, 54−60.
(41) Lustemberg, P. G.; Vericat, C.; Benitez, A.; Vela, E.; Tognalli, N.; Fainstein, A.; Martiarena, M. L.; Salvarezza, R. C. Spontaneously Formed Sulfur Adlayers on Gold in Electrolyte Solutions: Adsorbed Sulfur or Gold Sulfide? *J. Phys. Chem. C* **2008**, *112*, 11394−11402.
(42) O'Sullivan, C.; Gunning, R. D.; Barret, A.; Singh, A.; Ryan, K. M. Sized controlled gold tip growth onto II-VI nanorods. *J. Mater. Chem.* **2010**, *20*, 7875−7880.
(43) cp2k.org; VandeVondele, J.; Krack, M.; Mohamed, F.; Parrinello, M.; Chassaing, T.; Hutter, J. Quickstep: Fast and Accurate Density Functional Calculations Using a Mixed Gaussian and Plane

DOI: 10.1021/acs.chemmater.6b00287
Chem. Mater. 2016, 28, 2704−2714

Waves Approach. Comput. *Comput. Phys. Commun.* **2005**, *167*, 103−128.
(44) Halder, A.; Ravishankar, N. Gold Nanostructures from Cube-Shaped Crystalline Intermediates. *J. Phys. Chem. B* **2006**, *110*, 6595−6600.
(45) Mokari, T.; Costi, R.; Sztrum, C. G.; Rabani, E.; Banin, U. Formation of symmetric and asymmetric metal−semiconductor hybrid nanoparticles. *Phys. Status Solidi B* **2006**, *243*, 3952−3958.
(46) Khon, E.; Hewa-Kasakarage, N. N.; Nemitz, I.; Acharya, K.; Zamkov, M. Tuning the Morphology of Au/CdS Nanocomposites through Temperature-Controlled Reduction of Gold-Oleate Complexes. *Chem. Mater.* **2010**, *22*, 5929−5936.

DOI: 10.1021/acs.chemmater.6b00287
Chem. Mater. 2016, 28, 2704−2714